Atomistic Description of Interdroplet Ice-Bridge Formation during Condensation Frosting

Stefano Curiotto, David Paulovics, Christophe Raufaste, Franck Celestini, Thomas Frisch, Frédéric Leroy, Fabien Cheynis, Pierre Müller

this is a pre-print, the final version of the article has been published on Langmuir, https://doi.org/10.1021/acs.langmuir.2c02860

Atomistic description of interdroplet ice-bridge formation during condensation frosting

Stefano Curiotto,[*,†] David Paulovics,[‡] Christophe Raufaste,[‡,¶] Franck Celestini,[‡] Thomas Frisch,[‡] Frédéric Leroy,[†] Fabien Cheynis,[†] and Pierre Müller[†]

†*Aix Marseille University, CNRS, CINAM, Campus de Luminy, 13288 Marseille, France*
‡*Université Côte d'Azur, CNRS, Institut de Physique de Nice (INPHYNI), 06100 Nice, France*
¶*Institut Universitaire de France (IUF), 75005 Paris, France*

E-mail: stefano.curiotto@cnrs.fr

Abstract

The propagation of frost in an assembly of supercooled dew droplets takes place by the formation of ice protrusions that bridge ice particles and still-liquid droplets. In this work we develop a Kinetic Monte Carlo (KMC) model to study the formation kinetics of the ice protrusions. The KMC simulations reproduce well the experimental results reported in the literature. The elongation speed of the ice protrusions does not depend on the droplet size but increases when the inter-droplet distance decreases, the temperature increases or the substrate wettability increases. While 2D diffusion of the water molecules on the substrate surface is sufficient to explain the process kinetics, high 3D (vapor) water-molecules concentration can lead to development of 3D lateral branches on the ice protrusions. A 1D analytical model based on the water-molecules concentration gradient between a droplet and a nearby ice particle reproduces well the simulation results and highlights the relation between the protrusion elongation kinetics and parameters like the inter-droplet distance, the water diffusivity and the concentration gradient. The bridge-formation time has a quadratic dependence on the droplet-ice distance. Comparing the simulations, the analytical model and the experimental results of the literature we conclude that the propagation of frost on a flat substrate in an assembly of supercooled dew droplets with interdroplet spacing larger than about 1 micron is limited by water-molecule diffusivity.

Keywords: breath figures, atomistic simulations, dynamic evolution, dew droplets, frost propagation, condensation frosting, interdroplet ice bridge

Introduction

The uncontrolled formation of frost on materials surfaces can cause important damages in many components of different technologies. For instance, frost changes the aerodynamic behavior of aircraft wings[1], reduces the performances of heat pumps[2,3], can damage solar panels[4] and wind mills[5], can lead to asphalt road degradation and cause road accidents[6]. Understanding the formation of frost is thus of utmost importance and is still a challenge. It is generally admitted that the formation of frost on surfaces takes place in four steps: (i) condensation of supercooled liquid droplets from a moist environment, and droplet growth by coalescence[7]; an assembly of droplets on a surface is also known as "breath figure"[8]; (ii) random freezing of a droplet that becomes an ice particle; (iii) formation of ice protrusions (also called dendrites by some authors) from the frozen droplet to-

wards the nearest neighbors liquid droplets; (iv) when an ice protrusion reaches a liquid droplet, forming an ice bridge, the connected droplet freezes and the process restarts from step (iii). This process could also take place in 3D, in atmospheric supercooled clouds[9]. The in-plane propagation of frost was first observed by Dooley[10] and Guadarrama-Cetina et al.[9]. Petit and Bonaccurso studied the effect of the substrate stiffness on the frost formation, finding that polymer substrates can delay frost formation[11]. More recently, different modes of frost patterning have been uncovered using laser-induced fluorescence microscopy on micro-structured pillar arrays[12]. Paulovics et al. used thermal imaging to study the propagation of frost in breath figures[13]. They showed that the front propagation speed which was denoted as the percolation speed was a non-monotonous function of the droplet characteristic size. They found that the frost front propagation speed is defined by two characteristic time scales: the ice-bridge formation time and the freezing time of individual droplets (points (iii) and (iv) described above). Several advances in the comprehension of frost propagation have been made by Nath, Boreyko and coworkers[14–17]. With their experimental observations on droplets assemblies of 1 µm - 1 mm average diameter, they found that the kinetics of inter-droplet ice bridging depend on substrate wettability, temperature, and ambient humidity. However, the criterion for a protrusion to successfully form a bridge with a liquid droplet depends only on the inter-droplet distance and on the droplet size. They found that the bridge formation is due to the difference of saturation water pressure between an ice particle and a water droplet. This difference implies a concentration gradient of water molecules and thus a mass flux from the droplet to the ice particle: molecules evaporating from the droplet diffuse towards the frozen particle, stick there and form an ice protrusion.

Another mechanism of frost propagation has also been recently described in the literature for strongly hydrophobic surfaces[18]: when a supercooled droplet solidifies, the temperature increase due to recalescence leads to strong evaporation. In the dense propagating vapor front, microscopic ice crystals form; when they reach nearby supercooled droplets they act as nucleation sites and the droplets touched by the microscopic ice crystal freeze. This process might be important on structured, superhydrophobic rough surfaces like those used by Boinovich et al.[19], where ice protrusions are difficult to form. We do not investigate this mechanism, in the present work we focus on the formation of ice protrusions that bridge an ice particle with a liquid droplet, i.e. on point (iii) of the first frost-propagation process described above. The kinetics of bridge formation depend on the processes taking place at the nano scale. Kinetic Monte Carlo simulations (KMC) are ideally suited to tackle these issues. They allow the evaluation of different mechanism scenarios, for instance the relative importance of surface and gas diffusion on the ice bridge formation. Furthermore, in simulations it is possible to independently change physical parameters that are often difficult to separate experimentally, like the system temperature and the inter-droplet distance. Different geometrical configurations can also be easily achieved and systematically studied. Some authors have also used KMC simulations to study reactions[20].

In this article, we at first describe the KMC model used in the simulations. Then we detail the results of different simulations performed to prove the ability of our KMC model to reproduce the propagation of frost in an assembly of dew droplets. In a following section we discuss the kinetics of bridge formation between an ice front and a liquid droplet in the simulations. Then, we develop an analytical model able to explain the observed kinetics. Before concluding, the predictions of the simulations are compared with experimental results described in the literature.

Experimental

In our numerical experiments we use a simulation box where water/ice molecules can occupy positions of a 3D hexagonal close-packed (HCP) lattice. The total number of molecules in a simulation is constant. The model is similar to

that used in[21]. The molecules can jump from a position to a nearest neighbor empty position. Molecules of the first layer are in contact with a frozen substrate. The distance between two nearest neighbor positions is the lattice unit, taken as our unit of length equal to 1. The rate at which a water molecule jumps depends on the molecule binding energy, that is taken proportional to the number of nearest neighbors. The jump rate is $\nu_0 \exp[-(n\mathrm{J} - \delta E_S)/(kT)]$, where n is the number of nearest neighbors, J is a bond energy (it is taken as the energy unit in our system), k is the Boltzmann constant, T is the temperature, and ν_0 is the jump attempt frequency, that defines our time unit and is taken equal to 1 for all jumps. δ is equal to 1 for molecules in contact with the substrate and 0 in all other cases. The E_S term is necessary to take into account that the binding energies between water molecules are different from those between a molecule and the substrate. We have taken E_S=1, 2 and 2.99 J for hydrophilic, hydrophobic and strongly hydrophobic substrates respectively. For instance, for E_S=2 J, the effective jump energy of isolated water molecules on the substrate is $n\mathrm{J} - E_S$ = 3 J- 2 J = J (considering three bonds between the molecule and the substrate, $n = 3$). E_S represents an excess energy and defines the wetting properties between the substrate and the water molecules: a droplet wetting angle is $\theta' = \arccos(1 - \frac{2}{3}E_S)$ (for more information see the supplementary information in[21]). A molecule can sublimate, i.e. can detach from a droplet and jump to a position where it has no neighbors with a rate $\nu_0 \exp[-(n\mathrm{J} - \delta E_S + E_{evap})/(kT)]$, where E_{evap} is an additional evaporation energy. In our algorithm, at each KMC step a jump is executed and the time advances by the inverse of the sum of all jump rates, which allows obtaining correct time scales[22]. Molecules can diffuse on the substrate, on the droplets and in the vapor phase. Notice that, as the maximum E_S is 2.99 J, it is always energetically more favorable for molecules in the vapor phase to adsorb on the substrate than to stay in the vapor. A water molecule being part of an ice particle (ice molecule) can also displace but with smaller rate and thus in this case we take a bond energy J'>J. The simulation box has a roof from where gas molecules bounce back and planar periodic boundary conditions such that a molecule jumping out of the box from one side lands on the opposite side. The size of the simulation box is typically 500 (x) × 500 (y) × 25 (z) lattice units. The number of molecular moves is in the order of 10^9. The typical duration of a simulation on an Intel(R) Xeon(R) Silver 4216 CPU 2.10GHz is several hours. At each KMC step, if a water molecule has one or more ice molecules as neighbors, it becomes an ice molecule. Therefore within our KMC model, the kinetics of solidification inside a droplet touched by a bridge are very fast, are not meaningful and will not be discussed.

Results and discussions

Frost propagation: Qualitative predictions and KMC model validation

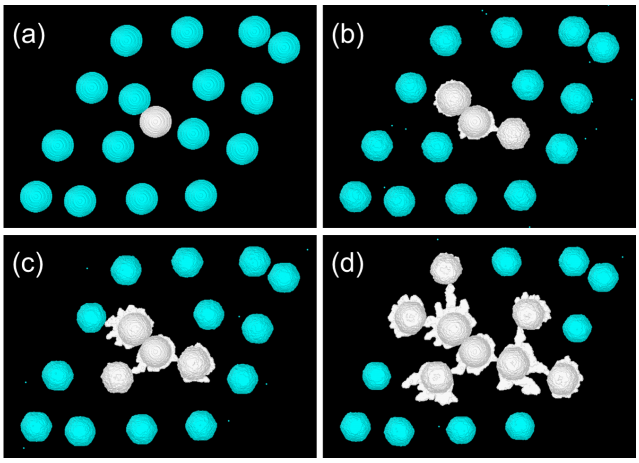

Figure 1: Snapshots of a simulation taken at successive times, extracted from movie S1, available in the supporting information. (a): starting configuraton with an ice particle (white) in the middle and 16 droplets (blue) randomly positioned around the ice particle; (b-d): the ice particle develops protrusions that elongate and form bridges with nearby droplets. When water droplets solidify, ice protrusions develop from their edges towards still-liquid droplets. kT = 0.5 J, E_S = J, E_{evap} = 5 J, J'=1.6 J.

Figures 1a-d show four snapshots of a simulation of the propagation of frost in a breath figure, the entire simulation is available in the

supporting information (Movie S1). In the figures, water and ice molecules are represented by small spheres colored in blue and white respectively. At the beginning of the simulation (figure 1a), a central ice particle is surrounded by liquid droplets positioned randomly on the surface. Water molecules detach from the droplets, randomly diffuse on the substrate, and can either re-attach to a liquid droplet or attach to an ice particle. Molecules of an ice particle are less mobile than those of a liquid droplet, they do not move much from the position where they have touched the ice particle and thus when molecules attach to frozen particles, ice protrusions start forming. Because of the detachment of water molecules and the formation of protrusions, liquid droplets shrink. Molecules detached from a droplet most probably attach to the closest ice particle, therefore ice protrusions form between nearby ice particles and droplets. When several ice particles are close to a same droplet, they all develop protrusions; however, the closest ice particle will develop protrusions faster. The protrusion reaching a droplet and forming a bridge is usually the one on the axis between the center of the droplet and the center of the closest ice particle, however also secondary, slowly-growing protrusions form. The longest protrusion, closer to the water droplet, captures more water molecules and thus acts as a screen for the shorter protrusions. When a droplet freezes, as water molecules detach much less from ice particles, the molecule concentration around the frozen droplet decreases. All the protrusions formed toward the frozen droplet stop growing and new protrusions start to form at the frozen-droplet edges directed towards liquid droplets (compare figures 1c and d). At long times, the shape of bridges can rearrange, generally become smoother and long bridges can also fragment by beading due to Rayleigh-Plateau instabilities. This beading is similar to that observed in solid state dewetting experiments and simulations[23]. The features of bridge formation described above have also been experimentally observed[9,13,16]. Thus the simulations reproduce well, qualitatively, the experimental results of the literature.

Changing the parameters used for the simulations, we have observed some changes in the bridge formation behavior. For a systematic study we have used a configuration with an ice rod and two droplets on each of the rod long sides. Each rod side represents the edge of a large ice particle. This configuration is used to approach the frost propagation experiments, where the bridge widths and the ice-particle curvatures are small with respect to the ice-particle size. Figures 2a-c show the starting configuration and two snapshots of a simulation where the droplets are close to the ice fronts. In the first simulation steps, protrusions form at the left and at the right of the ice rod, the longest ones are those closer to the droplets, while protrusions far from the droplet/ice-front axis (red dashes in figure 2a) are shorter. In following times, while protrusions far from the droplet stop growing, those closer to the droplets become bridges. As shown in figure 2c, more than one protrusion can almost simultaneously touch the droplet. The fastest protrusion reaching a droplet typically develops close to the droplet/ice axis, where the concentration gradient of water molecules is highest. As described for the frost propagation in breath-figures (figure 1), the fastest grow-

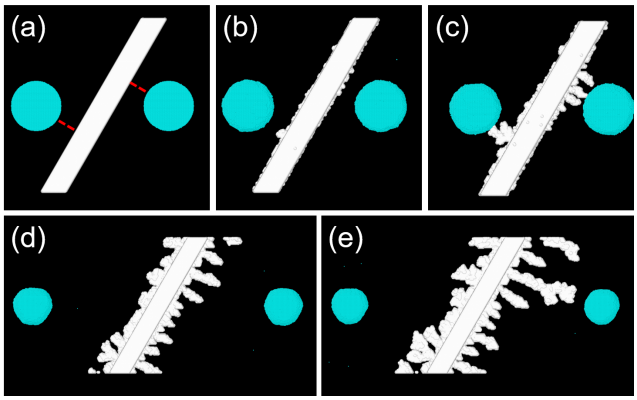

Figure 2: Snapshots of simulations of the frost propagation starting from an ice rod, white, and two water droplets, blue. The snapshots are taken at successive times. (a): configuration used at the beginning of a simulation where the droplets are close to the ice rod. The red dashed lines show the directions of shortest ice-droplet distance; (b): protrusions start forming along the ice edge; (c): some of the protrusions have reached the droplets and formed a bridge; (d-e): snapshots of a simulation where the ice-droplets distance is larger than for (a-c). $kT = 0.5$ J, $E_S =$ J, $E_{evap} = 5$ J, J'=2 J

ing protrusions capture more molecules than their neighbors that thus grow more slowly and eventually stop growing (screening effect). As shown in figure 2e, when the droplets are far from the ice front, the protrusions can also develop lateral branches.

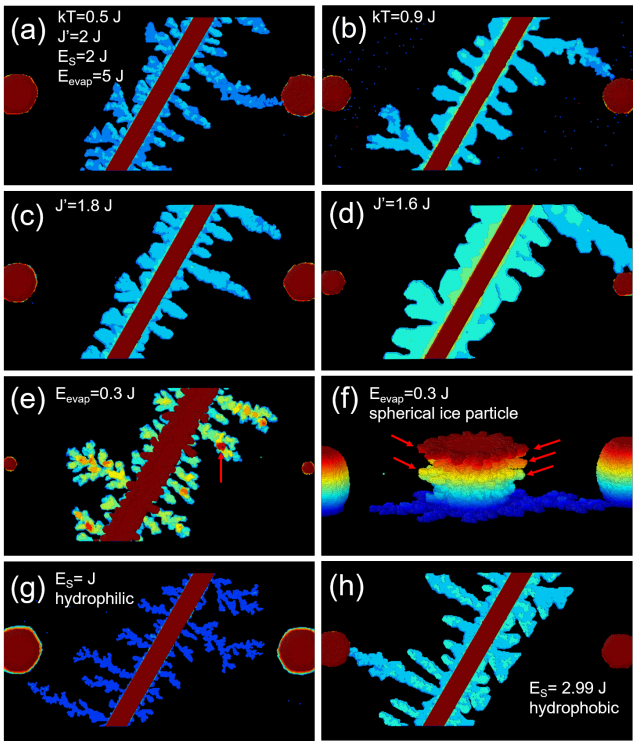

Figure 3: Snapshots of simulations with an ice rod that develops protrusions towards two water droplets. According to the parameters used in the simulations the protrusion shapes change. The color code refers to the molecule layer height: layers close to the substrate are colored in blue, and their color changes to light blue, green, yellow, orange and red when the protrusion height (in z) increases. The parameters used in (a) are directly written on the image. In all the other figures only the parameter that has changed with respect to (a) is shown. (a-b) show the effect of the temperature; the effect of the ice molecule binding energy J' can be evaluated by comparing (a), (c) and (d); the effect of the evaporation energy and thus of the vapor concentration is visible on (a) and (e) where the red arrow shows a vertical protuberance formed on the protrusion; (f) is a lateral view of a simulation with high evaporation to highlight the formation of lateral protrusions at different heights, marked with red arrows. For a better visualization we have used a spherical ice particle instead of an ice rod. The effect of the water/substrate wetting can be understood by comparing figures (a), (g) and (h) that show that the protrusion height increases when E_S (i.e. hydrophobicity) increases.

Figure 3 shows the effect of different parameters on the ice protrusions. In order to highlight the 3D shape of the protrusions, molecules close to the substrate are colored in blue, and their color changes to light blue, green, yellow, orange and red when the protrusion height (in z) increases. Molecules higher than 11 molecular layers are dark red. Figures 3a-b show that increasing the temperature, the protrusions are higher in z and their perimeter is smoother. Decreasing the ice/droplet bond energy ratio J'/J, the protrusions are higher in z, wider, and present less lateral branches (see figures 3c-d). As J'/J increases, the protrusions become more rough due to the fact that the detachment rate from the ice protrusions decreases and the edge diffusion along the protrusions also decreases. Figure 3e shows that increasing evaporation and thus the molecule concentration in the vapor (i.e. decreasing the evaporation energy), protruberances on top of the lateral ice protrusions form, like that pointed by a red arrow, while in figure 3a where evaporation and the molecule concentration in the gas are limited, the protrusion height is low and rather uniform. Furthermore, with high evaporation (and thus high concentration of molecules in the vapor that can condensate), lateral protrusions do not only form on the substrate, but also at different heights along the ice particle, as shown in figure 3f for a spherical ice particle (red arrows). Experimentally, as most observations are from the top of the samples, it is difficult to distinguish if the protrusions are only on the substrate; however our simulations show that the fastest protrusions are those developing on the substrate. We thus suggest that, even if evidently evaporation and gas diffusion take place, the main behaviors of bridge formation can be understood considering the diffusion of water molecules on the substrate surface. We have also carried out simulations with different wetting parameters E_S to study how the protrusion elongation changes when the substrate is hydrophilic, hydrophobic or strongly hydrophobic. Figure 3g shows that on hydrophilic substrates (good wetting, low E_S) the protrusions are thin and develop many branches. On hydrophobic substrates (bad wetting, high E_S) the thickness and the width of the ice bridges increase and their edges becomes smoother: Be-

cause of the increased hydrophobicity, ice wets and spreads less on the substrate, and tends to keep 3D shapes.

Because of the hexagonal crystallographic structure used in our KMC model, some ice surface orientations have lower energy than other orientations and are thus more stable. This takes place on orientations where the molecules have more neighbors, i.e. are more strongly bound. Therefore, ice protrusion edges in some directions can be more stable than others, and the protrusions can develop more in some directions (see for instance the difference between the protrusions developed on the left and on the right of the ice rod in figure 3h). This effect depends much on the parameters used in the simulations, and are particularly evident when the height of the protrusions is low. The threefold symmetry of ice islands of small height has also been observed by scanning tunneling microscopy[24,25] However, in experiments of frost propagation, where the bridges are thicker than a few molecular layers, shape and kinetic effects due to the ice crystallographic anisotropy probably cannot be observed and might be evidenced only at very low temperatures. In the discussion on the kinetics of bridge formation we neglect these anisotropy effects. In the simulations, thicker bridges with low anisotropy effects could be obtained by increasing the simulation box size and the number of molecular moves, but this is not possible in our KMC code because of memory allocation and computing time issues.

Kinetics of ice bridge formation

Figure 4a shows the length of the fastest ice protrusion reaching a droplet as a function of time, for three simulations where the initial ice-droplet distances are different. The time necessary to form a bridge increases with the ice-droplet distance. The protrusion length does not increase linearly with time, but accelerates close to the droplet, as experimentally observed by Petit and Bonaccurso[11]. Figure 4b compares the kinetics of protrusion elongation for simulations performed at different temperatures but keeping the initial ice-droplet distance constant. Increasing the temperature, protrusions form bridges faster. Notice that in experiments it is difficult to separately control temperature and interdroplet distance because at lower temperature more droplets nucleate from a moist atmosphere and thus the interdroplet distance is shorter than at higher temperature. Figure 4c shows that decreasing wetting (increase of hydrophobicity, increasing E_S), protrusions elongate more slowly, as also found by Boreyko and Collier[14] who explain that on superhydrophobic substrates the ice bridging is slow because the distance between droplets is high by virtue of the jumping-drop effect[14]. With our simulations we confirm that the time of bridge formation increases when the distance between droplets increases. Furthermore we also find that, for a same number of droplets per unit surface, the bridge formation on strongly hydrophobic substrates must be slower than on hydrophilic substrates. Changing the evaporation energy, i.e. changing the vapor pressure or equivalently the molecule concentration, the protrusion elongation kinetics are not significantly affected, as shown in figure 4d. We have also verified that the size of the water droplets does not affect the protrusion kinetics: We have measured a bridge-formation time of 1.23, 1.45 and 1.26 10^8 ν_0^{-1} for droplets with radius 12, 25 and 50 lattice units respectively (the kinetics of protrusion elongation are shown by the orange, red and blue circles in figure 4a for small, medium and large droplets respectively, the three data-sets are almost superposed). Our results do not confirm previous suggestions that the average bridge growth rate in a droplet population is inversely proportional to the average droplet size[17] and are in agreement with the observation of Paulovics et al.[13] that the bridge-formation time is independent from the droplets and ice particle size.

Concentration measurements

For some simulations, we have measured the concentration of water molecules on the substrate by counting the number of isolated molecules (without neighbors) in equilibrium with a water droplet, in the absence of ice. The

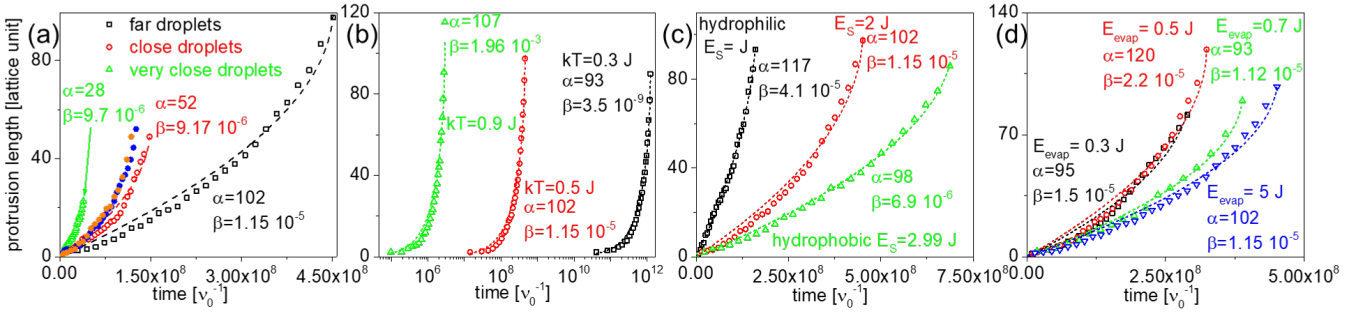

Figure 4: The four graphs show the length of the fastest ice protrusion as a function of time for different simulations. The data can be fitted with an expression developed in the section on the analytical model (see equation 5). The α and β parameters of this expression obtained from the curve fitting are given for each curve. (a): The curves show the protrusion elongation for droplets at 21 (very close), 50 (close) and 102 (far) unit lengths from the ice rod; The orange and the blue full circles represent simulations with droplet radius of 12 and 50 lattice units respectively, with the edge at 50 unit lengths from the ice rod; (b): Increasing the temperature the bridge forms faster; (c): On hydrophobic substrates the protrusion formation is slower; (d): Decreasing the evaporation energy in a simulation results in increasing the vapor pressure or equivalently the molecule concentration. However this does not seem to significantly affect the protrusion elongation kinetics. Unless otherwise specified, the simulation parameters are $kT = 0.5$ J, $E_S = 2$ J, J'=2 J, $E_{evap} = 5$ J, droplet radius: 25 lattice units

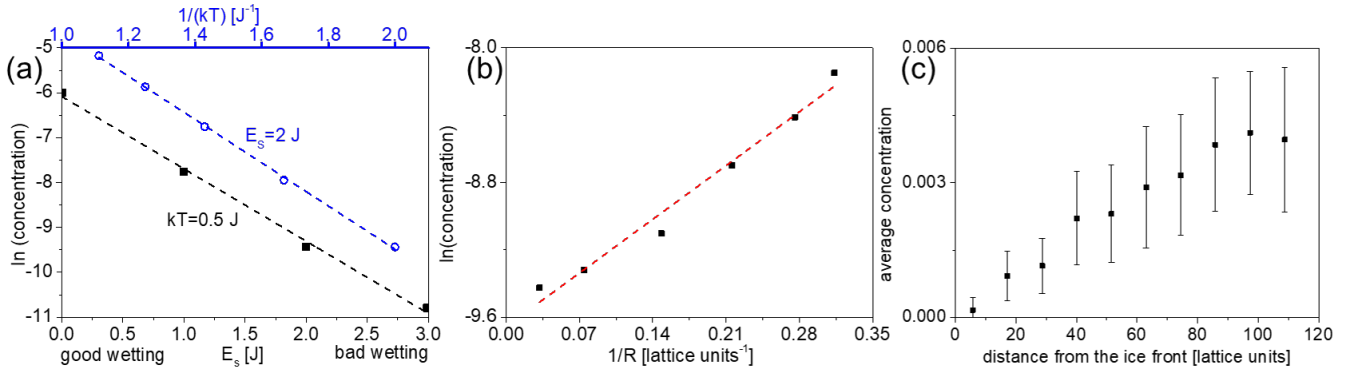

Figure 5: (a): The black squares show the natural logarithm of the water molecule concentration on the substrate (number of sites occupied by isolated molecules divided by the total number of sites on the substrate, excluded the sites occupied by the droplet) as a function of the parameter E_S (bottom x axis), for fixed kT=0.5 J. The blue circles show the natural logarithm of the concentration as a function of $1/(kT)$ for fixed E_S=2 J. For both datasets the droplet radius is large (31 lattice units) and the simulation box contains only a water droplet, no ice crystals. (b): natural logarithm of the concentration as a function of the inverse of the droplet radius; kT=0.5 J and E_S=2 J. (c): water molecule concentration between a water front and an ice front in the first stages of a simulation, before the protrusion formation, kT=0.9 J and E_S=2 J.

blue circles and the black squares in figure 5a show that the molecule concentration decreases when the temperature decreases and when E_S increases (i.e. when wetting decreases). Figure 5b shows that the molecule concentration increases when the droplet radius decreases. The concentration dependence on the temperature and on the droplet radius are due to the Gibbs-Thomson effect ($\ln(c) \propto \gamma/(kT \cdot R)$, where c is the concentration, γ the droplet surface energy and R the droplet radius[26]). The change of molecule concentration with the substrate wetting properties can be understood using the approach used in[27], and summarized in the supporting information S2. As regards the ice protrusions, within the range of parameters used in our simulations (strong binding energy), we have found that the molecule concentration around the ice phase is very low, and is negligible with respect to that around the liquid phase, also for very small curvatures of the ice phase. Therefore, in the simulations there is always a molecule concentration gradient between the liquid and the ice phase, and the pro-

trusion curvature does not affect it. In order to evaluate the concentration gradient between a droplet and an ice particle, we have averaged the number of molecules found at different distances between an ice front and a water front in the first stages of a simulation, before the formation of protrusions. The dispersion on the measurements is large, but the concentration profile, shown in figure 5c, confirms a decrease of water molecule concentration from the water front to the ice front.

Analytical model

Because of evaporation, molecules detach from water droplets and diffuse on the substrate or in the gas phase (3D volume around the droplets) before attaching to an ice particle. A molecule concentration gradient thus forms between a water droplet and the closest ice particle. This concentration gradient is the origin of the formation of the ice bridges. We develop here a simple analytical model in one dimension to describe how the protrusion tip position changes with time. The model, explained with the help of figure 6, is based on water molecules that detach from a droplet, diffuse, and attach to an ice particle. This approach has been employed in contexts different from frost propagation, particularly in surface diffusion studies (see as examples[28,29]).

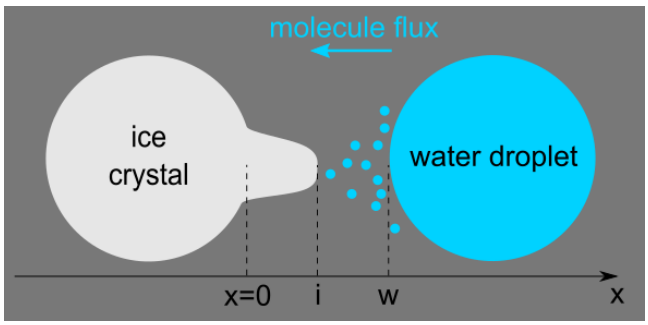

Figure 6: Position of the ice-protrusion (i), that depends on time, and of the water droplet edge (w), that is considered to be constant. The schematics is useful to understand the analytical model. Because of the molecule concentration gradient (higher concentration close to the droplet than close to the ice protrusion), a molecule flux from the droplet to the ice particle makes the protrusion grow.

The flux of molecules detaching from a water droplet is proportional to the difference between the concentration of molecules that would set up at equilibrium, in the absence of ice (C^{eq}_{drop}), and the real concentration at the water droplet edge, $C(x = w)$, with x the spatial coordinate between the droplet and the ice particle. The detaching flux of molecules can thus be written:

$$I_{det} = -K_{dr} \cdot (C^{eq}_{drop} - C(w)) \qquad (1)$$

where K_{dr} is a coefficient bound to the kinetics of molecules attachment and detachment at the water droplet edge. A concentration gradient sets up between the water droplet where molecules detach (high concentration) and the ice particle where the molecules attach (lower molecule concentration). For the first Fick's law, the diffusion flux in a concentration gradient is $I_d = -D\frac{dC(x)}{dx}$, where D is the diffusion coefficient. We assume a linear concentration gradient $C(x) = Ax + B$ where A and B can be found using the boundary condition $C(x) = C(w)$ at the droplet edge position $x = w$ and $C(x) = C(i)$ at the ice protrusion edge $x = i$. Therefore $A = \frac{C(i)-C(w)}{(i-w)}$ and the diffusive flux is

$$I_d = -D\frac{dC(x)}{dx} = -D\frac{C(w) - C(i)}{(w - i)} \qquad (2)$$

Notice that a linear concentration gradient can also be obtained in a quasi-steady state where the concentration gradient does not change with time t, because using the second Fick's law, $\frac{dC(x,t)}{dt}$=D$\frac{d^2C}{dx^2} = 0$. The flux of molecules attaching to the ice protrusion is, analogously to the detaching flux,

$$I_{att} = -K_i \cdot (C(i) - C^{eq}_{ice}) \qquad (3)$$

where K_i is a coefficient bound to the kinetics of molecules attachment and detachment at the ice edge and C^{eq}_{ice} is the equilibrium concentration of molecules around an isolated ice particle.

In a pure diffusive regime (negligible evaporation) the three fluxes must be equal and thus

we find:

$$I = I_{det} = I_d = I_{att} = \frac{C^{eq}_{ice} - C^{eq}_{drop}}{\frac{w-i}{D} + \frac{1}{K_i} + \frac{1}{K_{dr}}} \qquad (4)$$

In 1D each molecule arriving to the ice protrusion makes it advance by a length equal to the molecule dimension ℓ. Therefore the change of the protrusion tip position i with time depends on the flux written in equation 4: $\frac{di}{dt} = -I \cdot \ell$. Assuming that the droplet edge position does not significantly change with time, we consider w constant. This condition is always true for large droplets and it is not verified only for very small droplets. However, because of evaporation and detachment of molecules, small droplets often disappear before forming a bridge with an ice particle and thus the model would not apply anyway. Taking $\ell = 1$ as the unit length, $i(t = 0) = 0$ (notice that under this condition w corresponds to the starting ice-droplet distance), and solving the equation, leads to

$$\begin{aligned} i(t) &= \alpha - \sqrt{\alpha^2 - 2 \cdot \beta \cdot t} \\ \alpha &= D\left(\frac{1}{K_i} + \frac{1}{K_{dr}}\right) + w \\ \beta &= D \cdot \left(C^{eq}_{drop} - C^{eq}_{ice}\right) \end{aligned} \qquad (5)$$

Fitting the data of figures 4(a)-(d) with equation 5 using α and β as fitting parameters, we find a rather good agreement. The different values found for α and β are also reported in figure 4. In order to occasionally select also low-probability jump events, KMC simulations are based on random-numbers series. For a same set of KMC parameters but changing the random-number series, the α and β parameters are found to vary within 10 and 15% respectively. We find that α increases with the droplet-ice distance, as predicted by the definition of α given in equation 5. α does not depend much on the temperature because in our simulations $D(\frac{1}{K_i} + \frac{1}{K_{dr}}) << w$ (see later). The values of α found in the fits approximately correspond to the starting ice-droplet distances w (21, 50 and 102 unit lengths from the smaller to the larger distance). β does not depend much on w and increases with the temperature. In order to check if the values found are compatible with the definition of β given in equation 5, we have performed simulations to measure the number of isolated water molecules on the substrate for different temperatures in a simulation box containing only one water droplet, as shown by the blue circles in figure 5a. The measured molecule concentration is $1.6{\cdot}10^{-5}$ and $5.7{\cdot}10^{-3}$ for kT=0.5 and 0.9 J respectively (for kT=0.3 J the number of detached molecules is too small to define a concentration). C^{eq}_{ice} is negligible with respect to C^{eq}_{drop}. The diffusion coefficient on the substrate is $D = 1.5 \cdot exp\frac{-E_{diff}}{kT}$ (see[27]), with E_{diff} = J when E_S =2 J (3J-E_S=J, see the section on the KMC model) in our simulations. Therefore β should be about 10^{-3} and 10^{-5} for kT=0.9 and 0.5 J respectively, in agreement with the fitted values. The fitting parameters found are thus consistent with the physical meaning of α and β given in equation 5. Despite the several approximations, the 1D model developed above reproduces reasonably well the behavior of the ice bridge formation.

In our simulations we have found that the protrusion elongation is slower when wetting decreases (and thus the hydrophobicity increases). When wetting decreases, surface diffusion increases, and thus molecules detached from the water droplets reach faster the ice protrusion. However, when wetting decreases, molecules in contact with the substrate are less stable and thus their concentration decreases, as confirmed by our simulations of water molecule concentrations on the substrate for different wetting conditions, and shown in figure 5a.

The lower molecules concentration partially counterbalances the effect of faster diffusion on the velocity of protrusion elongation, but the concentration values that we find do not justify the reduced velocity of protrusion elongation. Actually, ice protrusions elongate slower when wetting decreases because their shape is more 3D, and their elongation on the substrate requires more water molecules.

The kinetics of protrusion elongation with strong evaporation does not significantly change with respect to simulations where only surface diffusion is present. Actually the difference between the protrusion elongation curves

in figure 4d is smaller than the difference obtained in simulations performed at different temperatures or for different ice-droplet distances (see figure 4a), and the α and β parameters that we find are within the 10 and 15 % dispersion discussed above.

Comparison with experimental results

The simulation results show that the ice-droplet distance w (corresponding to the final bridge length) and the time necessary to form a bridge have a sub-linear dependence, as shown in figure 7a. Our data can be compared with the ice-protrusion elongation studied by Paulovics et al.[13], under the hypothesis that the reservoir of water molecules in their work does not play an important role in the kinetics of a single ice-protrusion elongation. This assumption seems reasonable, because in the experimental study the ice protrusions are primarily fed by molecules coming from the water droplets, as proved by the directional growth of ice protrusions towards liquid droplets, and by the fact that protrusions stop growing in the absence of liquid droplets on the substrate. The inset of figure 7a, drawn using the data of reference[13], shows that the data points, originated from several slightly different experiments, are scattered, therefore they could be fitted with a straight line. However, from a single movie issued from that study (see movie S3 in the supporting information), we have measured the length of different ice protrusions as a function of time, as shown in figure 7b, finding that the behavior of the protrusion elongation corresponds to that obtained in the simulations. Using equation 5, the data sets of figure 7b are well fitted and we find an average β of $(6 \pm 2) \cdot 10^{-12}$ m^{2}s^{-1}. In our model the relations between the droplet-ice distance w and the time necessary for the bridge completion t_b can be found from equation 5 using the boundary condition $i(t = t_b) = w$:

$$w = -D \cdot (\frac{1}{K_i} + \frac{1}{K_{dr}}) + \\ + \sqrt{D^2 \cdot (\frac{1}{K_i} + \frac{1}{K_{dr}})^2 + 2\beta t_b} \quad (6a)$$

$$t_b = \frac{w}{C^{eq}_{drop} - C^{eq}_{ice}} \cdot (\frac{1}{K_i} + \frac{1}{K_{dr}} + \frac{w}{2D}) \quad (6b)$$

Equation 6a can be used to fit the bridge length as a function of t_b from the data sets of figure 7b (full blue line and right y axis in figure 7b).We find $\beta = (8 \pm 1) \cdot 10^{-12}$ m^{2}s^{-1}, that is consistent with the average value of β found above, and $D \cdot (\frac{1}{K_i} + \frac{1}{K_{dr}}) = (0.5 \pm 0.4)$ µm. Also the data reported in the inset of figure 7a could be better fitted with a sub-linear relation like that of equation 6a instead of a line (the sum of squared residuals is 11% lower with the sublinear relation than with a linear fit). Typical values of D for water molecules are in the order of 10^{-10} m^{2}s^{-1} (see[30]), therefore our measurements suggest a reasonable value for the concentration difference: $C^{eq}_{drop} - C^{eq}_{ice} = \beta/D \cong 10^{-2}$.

The different experimental data sets of figure 7b can be normalized by dividing $i(t)$ by w and the time by t_b. They are represented by the full symbols in figure 7c, where the data sets obtained by the simulations are also shown (empty symbols). Experimental and simulation results are well superposed. From equation 5, we obtain:

$$\frac{i(t)}{w} = (\epsilon + 1)\left(1 - \sqrt{1 - \frac{t}{t_b}\frac{2\epsilon + 1}{(\epsilon + 1)^2}}\right) \\ \text{with} \quad \epsilon = \frac{\alpha}{w} - 1 = \frac{D}{w}\left(\frac{1}{K_i} + \frac{1}{K_{dr}}\right) \quad (7)$$

The parameter ϵ is useful to compare D with $(\frac{1}{K_i} + \frac{1}{K_{dr}})$ over a length w. Equation 7 can be used to fit the datasets of figure 7c using ϵ as fitting parameter. In all cases we find $\epsilon \cong 0$, with no significant changes for the different datasets corresponding to different w. Therefore we can conclude that $D(\frac{1}{K_i} + \frac{1}{K_{dr}}) << w$ and thus the mechanism of frost propagation in breath figures is more limited by the water molecule diffusivity than by the kinetics of molecules attachment/detachment when the interdroplet

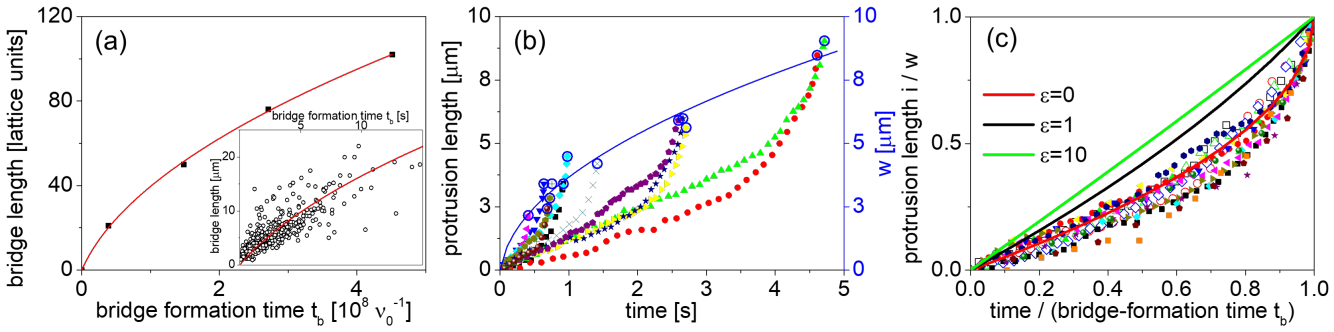

Figure 7: (a): Simulation (main figure) and experimental (inset) data of the dependence between the bridge length and the bridge formation time. The data of the inset are taken from[13]. A fit using equation 6a reproduces well the data. (b): The symbols represent the protrusion elongation as a function of time measured from an experimental movie of Paulovics et al.[13] for several bridge-formation events. The blue full curve is a fit of the bridge length versus the bridge-formation time (it should pass through the last symbol of each data set, marked with a blue empty circle) obtained using equation 6a. (c): The data of protrusion elongation versus time are normalized by dividing the protrusion length by w and the time by t_b. Full and empty symbols represent experimental and simulation results respectively. The full lines are drawn using equation 7 for different ϵ values.

spacing is larger than about 1 micron. Notice that the data of Petit and Bonaccurso[11] seem to be compatible with $\epsilon \approxeq 0$ suggesting that also in that work frost propagation is limited by molecule diffusivity. The simulations show that also for smaller interdroplet spacing the frost propagation is limited by water diffusion, however our KMC model does not take into account unknown (but possible) energy barriers to the attachment of water molecules to droplets and ice particles. On strongly hydrophobic substrates molecule diffusion is faster (large E_S and therefore high jump rates, see the section on the KMC model). In this case, as deduced from equation 6b for large D, it might be possible to observe linear relations between t_b and w[17] for small w, i.e. frost propagation might depend more on the attachment/detachment kinetics than on diffusivity.

Conclusions

We have shown that KMC simulations are perfectly suited to study the kinetics of bridge formation between an ice particle and a liquid droplet, important in the propagation of frost. Inter-droplet distance, temperature, and substrate wettability affect the kinetics of ice-bridge formation, while the droplet size does not change it. A 1D analytical model reproduces well the kinetics of the bridge formation mechanism, however we also observe some minor deviations because the ice particle, the droplet and the bridge between them are 3D. The analytical model can be used to analyze the experimental results of the literature. The time of formation of a single bridge has a quadratic dependence on the inter-droplet distance. With this analysis, we conclude that when the inter-droplet spacing is larger than about 1 micron, frost propagation in breath figures on flat substrates is limited by the water molecule diffusivity. As a future perspective it would be interesting to investigate the dynamics of ice-protrusion elongation on a micro-structured patterned surface in order to have a better understanding of frost formation on super-hydrophobic surfaces.

Associated Content

Supporting Information Movie S1 shows the KMC simulation of the propagation of frost in a breath figure (kT = 0.5 J, E_S=J, E_{evap} =5 J, J'=1.6 J, total time: $4.2{\cdot}10^8$ ν_0^{-1}). The pdf file S2 explains the dependence between the water molecule concentration on the substrate and the substrate wetting properties. Movie S3 shows the experimentally observed propagation of frost in a breath figure (image width 103 μm, total duration 9.7 s). This material is available free of charge via the Internet at http://pubs.acs.org.

Acknowledgments

We acknowledge the Doeblin federation for financial support. We thank O. Pierre-Louis for fruitful discussions.

References

(1) Broeren, A. P.; Lee, S.; Clark, C. Aerodynamic Effects of Anti-Icing Fluids on a Thin High-Performance Wing Section. *J. Aircraft* **2016**, *53*, 451.

(2) Song, M.; Dang, C.; Higashi, T.; Hihara, E. *Energy Build.* **2020**, *223*, 110103.

(3) Wang, W.; Xiao, J.; Guo, Q.; Lu, W.; Feng, Y. Field test investigation of the characteristics for the air source heat pump under two typical mal-defrost phenomena. *Appl. Energy* **2011**, *88*, 4470.

(4) Wang, D.; Huo, X.; Liu, Y.; Chen, Y.; Fan, B.; Xu, T.; Wang, L. A study on frost and high-temperature resistance performance of supercooled phase change material-based flat panel solar collector. *Sol. Energy Mater. Sol. Cells* **2022**, *239*, 111665.

(5) Wallenius, T.; Lehtomaki, V. Overview of cold climate wind energy: challenges, solutions, and future needs. *WIREs Energy Environ.* **2016**, *5*, 128.

(6) Tarpoudi Baheri, F.; Poulikakos, L.; Poulikakos, D.; Schutzius, T. Dropwise condensation freezing and frosting on bituminous surfaces at subzero temperatures. *Constr. Build. Mater.* **2021**, *298*, 123851.

(7) Beysens, D. *The Physics of Dew, Breath Figures and Dropwise Condensation*; Lecture Notes in Physics; Springer, Cham, 2022; Vol. 994; p 51.

(8) Spurr, R. T.; Butlin, J. G. Breath Figures. *Nature* **1957**, *179*, 1187.

(9) Guadarrama-Cetina, J.; Mongruel, A.; Gonzales-Vinas, W.; Beysens, D. Percolation-induced frost formation. *EPL* **2013**, *101*, 16009.

(10) Dooley, J. B. *Determination and characterization of ice propagation mechanisms on surfaces undergoing dropwise condensation*; PhD thesis Texas A & M University, 2010.

(11) Petit, J.; Bonaccurso, E. General frost growth mechanism on solid substrates with different stiffness. *Langmuir* **2014**, *30*, 1160.

(12) Hauer, L.; Wong, W. S. Y.; Sharifi-Aghili, A.; Kondic, L.; Vollmer, D. Frost spreading and pattern formation on microstructured surfaces. *Phys. Rev. E* **2021**, *104*, 044901.

(13) Paulovics, D.; Raufaste, C.; Frisch, T.; Claudet, C.; Celestini, F. Dynamics of Frost Propagation on Breath Figures. *Langmuir* **2022**, *38*, 2972.

(14) Boreyko, J. B.; Collier, C. Delayed Frost Growth on Jumping-Drop Superhydrophobic Surfaces. *ACS Nano* **2013**, *7*, 1618.

(15) Boreyko, J. B.; Srijanto, B.; Nguyen, T.; Vega, C.; Fuentes-Cabrera, M.; Collier, C. Dynamic Defrosting on Nanostructures Superhydrophobic Surfaces. *Langmuir* **2013**, *29*, 9516.

(16) Nath, S.; Ahmadi, S.; Boreyko, B. A Review of Condensation Frosting. *Nanoscale Microscale Thermophys. Eng.* **2017**, *21*, 81.

(17) Nath, S.; Ahmadi, S.; Boreyko, B. How ice bridges the gap. *Soft Matter* **2020**, *16*, 1156.

(18) Graeber, G.; Dolder, V.; Schutzius, T. M.; Poulikakos, D. Cascade Freezing of Supercooled Water Droplet Collectives. *ACS Nano* **2018**, *12*, 11274.

(19) Boinovich, L. B.; Emelyanenko, K. A.; Emelyanenko, A. M. Superhydrophobic versus SLIPS: Temperature dependence and the stability of ice adhesion strength. *J. Colloid Interface Sci.* **2022**, *606*, 556.

(20) Kurganskaya, I.; Luttge, A. Kinetic Monte Carlo Approach To Study Carbonate Dissolution. *J. Phys. Chem. C* **2016**, *120*, 6482.

(21) Curiotto, S.; Chame, A.; Müller, P.; Thompson, C. V.; Pierre-Louis, O. Hole opening from growing interfacial voids: A possible mechanism of solid state dewetting. *Appl. Phys. Lett.* **2022**, *120*, 091603.

(22) Voter, A. F. *Radiation Effects in Solids*; Springer, NATO Publishing Unit: Dordrecht, The Netherlands, 2005; p 4.

(23) Trautmann, M.; Cheynis, F.; Leroy, F.; Curiotto, S.; Pierre-Louis, O.; Müller, P. Dewetting of patterned solid films: Towards a predictive modelling approach. *Appl. Phys. Lett.* **2017**, *110*, 263105.

(24) Nie, S.; Bartelt, N. C.; Thürmer, K. Evolution of proton order during ice-film growth: An analysis of island shapes. *Phys. Rev. B* **2011**, *84*, 035420.

(25) Thürmer, K.; Nie, S. Formation of hexagonal and cubic ice duringlow-temperature growth. *PNAS* **2013**, *110*, 11757.

(26) Krishnamachari, B.; McLean, J.; Cooper, B.; Sethna, J. Gibbs-Thomson formula for small island sizes: Corrections for high vapor densities. *Phys. Rev. B* **1996**, *54*, 8899.

(27) Curiotto, S.; Müller, P.; Cheynis, F.; Leroy, F. Kinetic Monte Carlo simulations of the diffusion and shape evolution of single-layer clusters on a hexagonal lattice with and without external force. *Appl. Surf. Sci.* **2021**, *552*, 149454.

(28) McLean, J. G.; Krshnamachari, B.; Peale, D. R.; Chason, E.; Sethna, J. P.; Cooper, B. H. Decay of isolated surface features driven by the Gibbs-Thomson effect in an analytic model and a simulation. *Phys. Rev. B* **1997**, *55*, 1811.

(29) Curiotto, S.; Leroy, F.; Cheynis, F.; Müller, P. Reflections on the effect of an external flux in surface physics. *Surf. Sci.* **2022**, *725*, 122158.

(30) Park, J. H.; Aluru, N. D. Diffusion of water submonolayers on hydrophilic surfaces. *Appl. Phys. Lett.* **2008**, *93*, 253104.